

Chapter 3

Multiple Parton Interactions

By the fact that the hadrons are viewed as "bunches" of partons, it is likely that in the same hadron-hadron collision different couples of partons can undergo to a scattering. This phenomenon is known as *Multiple Parton Interactions* (MPI) and it is related to the composite nature of the incoming hadrons.

So, it is clear that at some level these MPI have to exist, and they can become important in the description of the event; they can change the color topology of the colliding system as a whole.

In this scenario it is important to have a good understanding of the phenomenon. The aim of this section is to describe the basic concepts that are use to simulate MPI, for example in *Pythia* Monte Carlo event generator; than some focus is given to the free parameters we are going to tune in the following sections.

3.1 Basic Concepts

The main hypothesis of the multiple interactions models is that: the QCD factorization theorem is true not only for the hard process but also for the other partons scatters.

So, we can write:

$$\frac{d\sigma_{\text{int}}}{dp_{\perp}} = \sum_{i,j,k,l} \int dx_1 \int dx_2 \int d\hat{t} f_i(x_1, Q^2) f_j(x_2, Q^2) \frac{d\hat{\sigma}_{ij \rightarrow kl}}{d\hat{t}} \delta\left(p_{\perp}^2 - \frac{\hat{t}\hat{u}}{\hat{s}}\right) \quad . \quad (3.1)$$

This represent the interaction differential cross section for the hadron-hadron collisions, where $\frac{d\hat{\sigma}_{ij \rightarrow kl}}{d\hat{t}}$ is the differential cross section for QCD hard $2 \rightarrow 2$ processes, this processes are the one reported in Table 3.1.

In Eq. 3.1 we used the Mandelstam variables associated to the partonic system:

$$\hat{s} = (p_1 + p_2)^2 = (p_3 + p_4)^2 = x_1 x_2 s \quad (3.2)$$

$$\hat{t} = (p_1 - p_3)^2 = (p_2 - p_4)^2 \quad (3.3)$$

$$\hat{u} = (p_1 - p_4)^2 = (p_2 - p_3)^2 \quad (3.4)$$

where p_1, p_2 are the four-momenta of the incoming partons and p_3, p_4 the four-momenta of the outgoing partons.

Note that in Eq. 3.1 the jet cross section is twice as large $\sigma_{\text{jet}} = 2\sigma_{\text{int}}$, because at first approximation each interaction gives rise to two jets.

We assume also that the "hardness" of processes is defined by the p_T scale of the interaction ($Q^2 = p_T^2$).

As you can see from the formulae in Table 3.1 at small scattering angles, for $t \rightarrow 0$, the t-channel gluon exchange processes $qq' \rightarrow qq'$, $qg \rightarrow qg$ and $gg \rightarrow gg$ dominate the full matrix element. For scatterings that are soft relative to \hat{s} , $|\hat{t}| \ll \hat{s}$, we can approximate $|\hat{t}|$ as:

$$p_T^2 = \frac{\hat{t}\hat{u}}{\hat{s}} = \frac{\hat{t}(-\hat{s} - \hat{t})}{\hat{s}} \approx |\hat{t}| \quad , \quad (3.5)$$

in this limit, the only differences between quark and gluon cross sections are the color factors

$$\hat{\sigma}_{gg} : \hat{\sigma}_{qg} : \hat{\sigma}_{qq} = \frac{9}{4} : 1 : \frac{4}{9} \quad . \quad (3.6)$$

So, the Eq. 3.1 can be rewritten like

$$\frac{d\sigma_{int}}{dp_T^2} \approx \int \int \frac{dx_1}{x_1} \frac{dx_2}{x_2} F(x_1, p_T^2) F(x_2, p_T^2) \frac{d\hat{\sigma}_{2 \rightarrow 2}}{dp_T^2} \quad , \quad (3.7)$$

whit:

$$\frac{d\hat{\sigma}_{2 \rightarrow 2}}{dp_T^2} = \frac{8\pi\alpha_s^2(p_T^2)}{9p_T^4} \quad ; \quad (3.8)$$

$$F(x, Q^2) = \sum_q (x q(x, Q^2) + x \bar{q}(x, Q^2)) + \frac{9}{4} x g(x, Q^2) \quad . \quad (3.9)$$

Now, we can integrate the Eq. 3.7:

$$\sigma_{int}(p_{Tmin}) = \int_{p_{Tmin}^2}^{(\sqrt{s}/2)^2} \frac{d\hat{\sigma}_{2 \rightarrow 2}}{dp_T^2} dp_T^2 \propto \frac{1}{p_{Tmin}^2} \xrightarrow{p_{Tmin} \rightarrow 0} \infty \quad (3.10)$$

The total cross section is divergent in the limit $p_T \rightarrow 0$, this divergence is shown in Fig. 3.1. Due to this divergence the total interaction cross section at some p_T scale can exceed the total proton-proton cross section.

To understand this paradox should be noted that the interaction cross section described in Eq. 3.10 is related to the interaction probability between two partons and counts the number of interactions, while the total proton-proton cross section σ_{pp} counts the number of events. For example, an event (a proton-proton collision) in which two partons interact counts once in the total cross section and twice in the interaction cross section.

So, the ratio between this two quantities is perfectly allowed to be larger than unity, we can write it down as:

$$\frac{\sigma_{int}(p_{Tmin})}{\sigma_{tot}} = \langle n \rangle(p_{Tmin}) \quad . \quad (3.11)$$

Furthermore, we have to consider the *screening effect*: in fact the incoming hadrons are color singlet objects. Therefore, when the p_T of an exchanged gluon is small, and so the associated wavelength large, this gluon cannot longer resolve the color charges and the effective coupling is decreased, this screening set a cutoff in the divergence. The screening effect is schematically shown in Fig. 3.2.

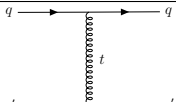
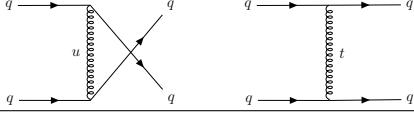
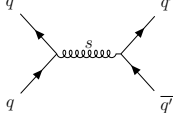
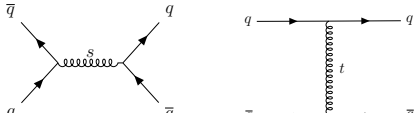
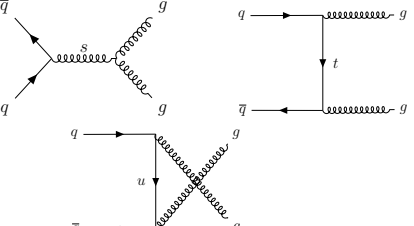
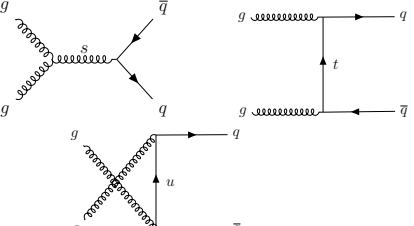
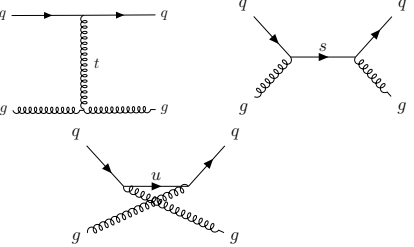
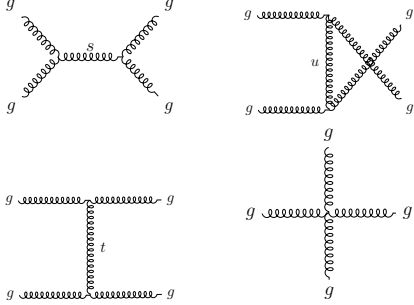
Process	Amplitude	$\sum \mathcal{M} ^2 / (4\pi\alpha_s)^2$
$qq' \rightarrow qq'$		$\frac{4}{9} \frac{s^2 + u^2}{t^2}$
$qq \rightarrow qq$		$\frac{4}{9} \frac{s^2 + u^2}{t^2} + \frac{4}{9} \frac{s^2 + t^2}{u^2} - \frac{8}{27} \frac{s^2}{tu}$
$q\bar{q} \rightarrow q'\bar{q}'$		$\frac{4}{9} \frac{t^2 + u^2}{s^2}$
$q\bar{q} \rightarrow q\bar{q}$		$\frac{4}{9} \frac{s^2 + u^2}{t^2} + \frac{4}{9} \frac{t^2 + u^2}{s^2} - \frac{8}{27} \frac{u^2}{st}$
$q\bar{q} \rightarrow gg$		$\frac{32}{27} \frac{t^2 + u^2}{tu} - \frac{8}{3} \frac{t^2 + u^2}{s^2}$
$gg \rightarrow q\bar{q}$		$\frac{1}{6} \frac{t^2 + u^2}{tu} - \frac{3}{8} \frac{t^2 + u^2}{s^2}$
$qg \rightarrow qg$		$-\frac{4}{9} \frac{s^2 + u^2}{su} + \frac{s^2 + u^2}{t^2}$
$gg \rightarrow gg$		$\frac{9}{2} \left(3 - \frac{tu}{s^2} - \frac{su}{t^2} - \frac{st}{u^2} \right)$

Table 3.1: Parton-Parton differential cross sections ($2 \rightarrow 2$ QCD process), can be calculated in pQCD evaluating the matrix element for each process involving quark, antiquark and gluon. Table from [26]

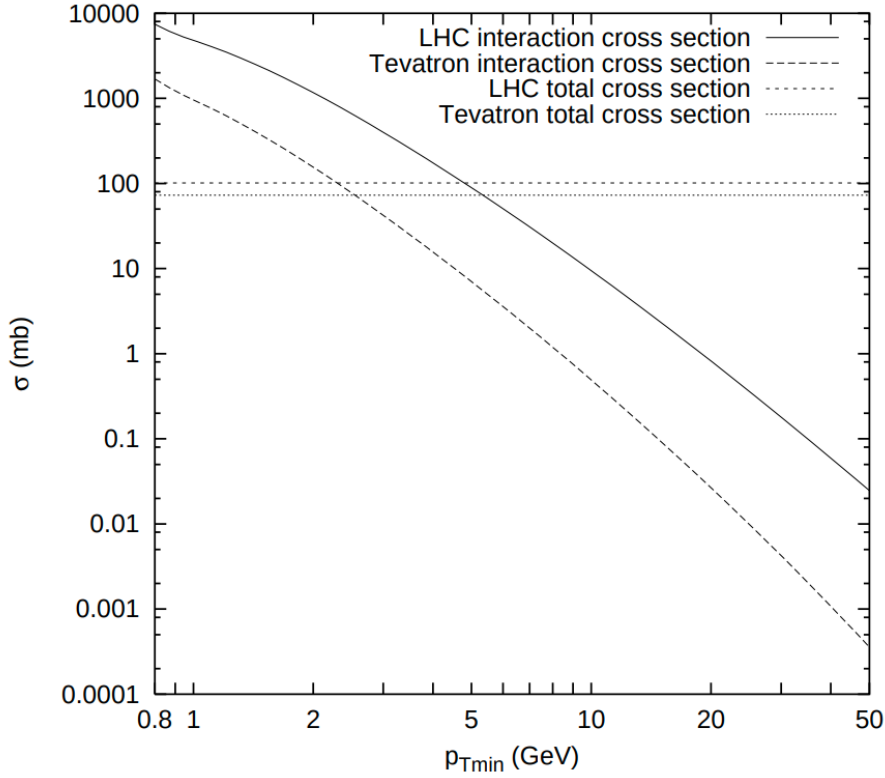


Figure 3.1: This figure shows the interaction cross section (σ_{int}) at Tevatron ($p\bar{p}$, $\sqrt{s} = 1.8$ TeV) and at LHC (pp , $\sqrt{s} = 14$ TeV). The flat lines are the corresponding values for the total cross section. The interaction cross section that arise from Eq. 3.10 is divergent for $p_{T\min} \rightarrow 0$ in reality a dumping of this divergence is expected due to the color screening effect.

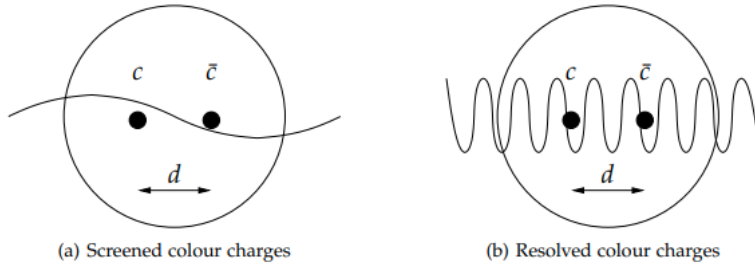


Figure 3.2: A picture of the screening effect. The left figure show two color charge that are not resolved by the gluon in fact the wave length is greater than the spatial separation, d , of the two charges. So resolution of the probe is not enough to discriminate the color charges. While on the right figure the two charges are very well distinct.

So, this cutoff is associated with color screening distance i.e. the average size of the region within the compensation of color charge occurs. This cutoff is then introduced in the factor as:

$$\frac{\alpha_s^2(p_{T0}^2 + p_T^2)}{\alpha_s^2(p_T^2)} \frac{p_T^4}{(p_{T0}^2 + p_T^2)^2} \quad (3.12)$$

This factor contains the phenomenological regularization of the divergence, with the factor p_{T0} that have to be tuned to data.

Now the interaction cross section is smoothly regularized and therefore finite.

To be notice that: parameter p_{T0} do not have to be energy-independent, but since the energy is related with the sensibility of our probe, higher energy is related with the capacity of probing PDFs to lower x values (as discussed previously, see Fig. 2.7) and in this low x region the number of partons rapidly increases. So, the partons are closer packed in this regions and as a consequence the color screening distance decrease.

The number of partons is related to x with a power law so, it is likely to have a dependence of the same form for p_{T0} respect to the center-of-mass energy

$$p_{T0}(\sqrt{s}) = p_{T0}^{ref} \left(\frac{\sqrt{s}}{E_{CM}^{ref}} \right)^{E_{CM}^{pow}}. \quad (3.13)$$

In the next section we are going to discuss how this and other effects fit into the Monte Carlo generator pythia8.

3.2 Pythia8 Monte Carlo events generator

Pythia8 is a standard tool for the simulation of events in high energy collisions. Pythia contains the evolution from a few-body system to a complex multiparticles final state.

3.2.1 Parton Shower

In Pythia8 all the contributions from Initial State Radiation (ISR), Final State Radiation (FSR) and Multi Parton Interactions (MPI) are interleaved into a single common sequence of decreasing p_T .

The parton shower has been described in the previously section. The solution to the DGLAP equation is given putting Eq. 2.12 and Eq. 2.13 in Eq. 2.14 for the ISR and the FSR by a Sudakov form factor that is related to the no emission probability in the p_T -evolution.

The evolution variables for ISR and FSR are defined starting from the virtuality (Q^2) of the emission:

$$p_T^2 = \begin{cases} (1-z)Q^2 & \text{ISR} \\ z(1-z)Q^2 & \text{FSR} \end{cases}, \quad (3.14)$$

so, in the two cases: for the FSR $Q_{FSR}^2 = (p^2 - m_0^2)$ in fact a time-like virtuality ($p^2 > 0$) is implicated, while for the ISR we have $Q_{ISR}^2 = (-p^2 + m_0^2)$ with a space-like virtuality ($p^2 < 0$). In both case Q^2 values are positive defined. Than the actual strong of the radiation is set by the choices of $\alpha_{s\,ISR}$ and $\alpha_{s\,FSR}$ values.

3.2.2 Multiple Parton Interactions in Pythia

The MPI, as said before, are also generated in a decreasing p_T sequence. So the hardest MPI is generated first. Than we can write the probability for an interaction, i , to occur at a scale p_T using a Sudakov-type expression (as we have done for the

ISR and the FSR):

$$\frac{d\mathcal{P}_{MPI}}{dp_T} = \frac{1}{\sigma_{ND}} \frac{d\sigma_{2 \rightarrow 2}}{dp_T} \exp \left(- \int_{p_T}^{p_T^{i-1}} \frac{1}{\sigma_{ND}} \frac{d\sigma_{2 \rightarrow 2}}{dp'_T} dp'_T \right) . \quad (3.15)$$

3.2.3 Momentum and flavour conservation

One problem is to achieve momentum conservation, so we need to take into account the modification in the PDF by the $i-1$ interaction. To do that in `Pythia` the PDF are rescaled to the remaining available x range, adjusting their normalization.

We need to take into account the momentum fraction x_i removed from the hadron remnant by the $i-th$ interaction. This is done evaluating PDF not at x_i but at a rescaled value

$$x'_i = \frac{x_i}{X} \quad \text{with} \quad X = 1 - \sum_{j=1}^{i-1} x_j . \quad (3.16)$$

So, using these quantities, we can rewrite our PDFs as:

$$f_i(x, Q^2) \longrightarrow \frac{1}{X} f_0 \left(\frac{x}{X} \right) , \quad (3.17)$$

where f_0 is the original one-parton inclusive PDFs.

Now, requiring also the flavour conservation and taking into account the number of valence and/or sea quarks involved in the preceding MPI. We have now the full forms of the PDFs used for the $i-th$ MPI:

$$f_i(x, Q^2) = \frac{N_{fv}}{N_{fv0}} \frac{1}{X} f_{v0} \left(\frac{x}{X}, Q^2 \right) + \frac{a}{X} f_{s0} \left(\frac{x}{X}, Q^2 \right) + \sum_j \frac{1}{X} f_{cj0} \left(\frac{x}{X}, Q^2 \right) , \quad (3.18)$$

$$g_i(x, Q^2) = \frac{a}{X} g_0 \left(\frac{x}{X}, Q^2 \right) , \quad (3.19)$$

where:

- $f_i(x, Q^2)$ ($g_i(x, Q^2)$) are the squeezed PDFs for quarks (gluons);
- N_{fv} the number of remaining valence quarks of the given flavour;
- N_{fv0} the number of original valence quarks of the given flavour (for the proton we have $N_u = 2$, $N_d = 1$);
- f_{s0} the sea-quark PDF;
- f_{cj} the companion PDF, this arise from the splitting $g \rightarrow q\bar{q}$ and a quark j is kicked out.

The factor a is defined to satisfy the total momentum sum rule.

3.2.4 Impact Parameter Dependence

The simplest hypothesis for the multiple interaction simulation, it is to assume the same initial state for all hadron collisions without dependencies on the impact parameter.

The more realistic scenario it is to include the possibility that each collision could be characterized by a different impact parameter b , where a small b value correspond to a large overlap between the two hadrons this is related to the probability of parton-parton interaction to take place.

To include the impact parameter dependence on the collision, it is necessary to make some assumption on the matter distribution inside the proton. A possibility is to assume a spherically symmetric distribution inside an hadron at rest $\rho(\mathbf{x}) d^3x = \rho(r) d^3x$. A Gaussian ansatz is the most simple choice but it appears to lead to a narrow multiplicity distribution and a too little pedestal effect. So the choice is a double Gaussian:

$$\rho(r) \propto \frac{1-\beta}{a_1^3} \exp\left\{-\frac{r^2}{a_1^2}\right\} + \frac{\beta}{a_2^3} \exp\left\{-\frac{r^2}{a_2^2}\right\} \quad , \quad (3.20)$$

where a fraction β of matter is contained in a radius a_2 , and the rest in a larger radius a_1 .

Now, for a given matter distribution $\rho(r)$, the time-integrated overlap function of the incoming hadrons during the collision is given by:

$$\mathcal{O}(b) = \int dt \int d^3x \rho(x, y, z) \rho(x+b, y, z+t) \quad . \quad (3.21)$$

Assuming the matter distribution function in Eq. 3.20 and inserting it into Eq. 3.21 we get the following expression.

$$\mathcal{O}(b) \propto \frac{(1-\beta)^2}{2a_1^2} \exp\left\{-\frac{b^2}{2a_1^2}\right\} + \frac{2\beta(1-\beta)}{a_1^2 + a_2^2} \exp\left\{-\frac{b^2}{a_1^2 + a_2^2}\right\} + \frac{\beta^2}{2a_2^2} \exp\left\{-\frac{b^2}{2a_2^2}\right\} \quad (3.22)$$

this is useful to quantify the effect of overlapping protons. The larger is $\mathcal{O}(b)$ the more probable are parton-parton scatters between the incoming protons $\langle \tilde{n} \rangle \propto \mathcal{O}(b)$.

So, these assumption change the so-far Poissonian nature of the framework¹

$$\mathcal{P}(\tilde{n}) = \langle \tilde{n} \rangle^{\tilde{n}} \frac{e^{-\langle \tilde{n} \rangle}}{\tilde{n}!} \quad (3.23)$$

Now the request that at least one parton interactions in the hadron-hadron collision, ensures that we get a finite total cross section. So the probability that an event is produced by two hadrons scattering with impact parameter b :

$$\mathcal{P}_{\text{int}} = \sum_{\tilde{n}=1}^{\infty} \mathcal{P}_{\tilde{n}(b)} = 1 - \mathcal{P}_0 = 1 - e^{-\langle \tilde{n}(b) \rangle} = 1 - e^{-k\mathcal{O}(b)} \quad (3.24)$$

¹the Poissonian distribution, in Eq. 3.23 describe the probability of having n interactions at each impact parameter. If the matter distribution have an infinite tail (like our in Eq. 3.20) events may be obtained with arbitrarily large b values. This can be a problem for the definition of the total hadron-hadron cross section

So we have now that the number of interaction per event is give by (for impact parameter b):

$$\langle n(b) \rangle = \frac{\langle \tilde{n}(b) \rangle}{\mathcal{P}_{\text{int}}} \quad (3.25)$$

so, this have modified the probability distribution of interactions number from a Poissonian to a narrower one at each b fixed.

3.2.5 Parton rescattering

It is not necessary that the partons undergoing to a MPI are a different partons couple from the one scattered before. As shown in Fig. 3.3 MPI can also arise when a parton scatters more than once against partons from the other beam, this is call *parton rescattering*.

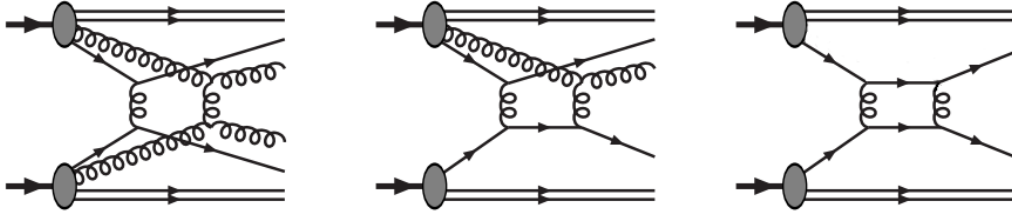


Figure 3.3: This figure shows parton rescattering. On the right image a double $2 \rightarrow 2$ scattering (no rescattering) is shown; on the middle a parton rescattering process where only one of the rescattered partons have already scattered; on the right image a parton rescattering with both the partons that undergo to rescattering have already been scattered.

We can have 3 type of MPI:

1. No ones of the partons that enter in the second scattering undergoes to another scatter before (Fig. 3.3 left);
2. Only one of the two partons has already been scattered (Fig. 3.3 middle);
3. Both the partons have already been scattered before (Fig. 3.3 right).

The second and the third are the rescatters the overall influence of rescatters in proton-proton interactions was estimated to be small respect to the first case with distinct $2 \rightarrow 2$ scatters.

The simulation of parton rescatters start from the evaluation of the parton density as:

$$f(x, Q^2) \longrightarrow \underbrace{f_{\text{rescaled}}(x, Q^2)}_{\text{hadron remnant}} + \underbrace{\sum_n \delta(x - x_n)}_{\text{scattered parton(s)}} \quad , \quad (3.26)$$

where the $\delta(x - x_i)$ takes into account the already scattered partons that have a fixed momentum fraction x_n . While the hadron remnant is still described by a continuous momentum density, scaled to achieve momentum conservation:

$$\int_0^1 \left(f_{\text{rescaled}}(x, Q^2) + \sum_n \delta(x - x_n) \right) dx = 1 \quad . \quad (3.27)$$

3.2.6 Interleaving of Multiple Interaction and Parton Shower

As discussed above the MPI are simulated in `Pythia` following a decreasing p_T evolution. So we have that the total probability is given from the composition of the various contributions:

$$\frac{d\mathcal{P}}{dp_T} = \left(\frac{d\mathcal{P}_{MPI}}{dp_T} + \sum \frac{d\mathcal{P}_{ISR}}{dp_T} + \sum \frac{d\mathcal{P}_{FSR}}{dp_T} \right) \times \exp \left\{ - \int_{p_T}^{p_T^{i-1}} \left(\frac{d\mathcal{P}_{MPI}}{dp'_T} + \sum \frac{d\mathcal{P}_{ISR}}{dp'_T} + \sum \frac{d\mathcal{P}_{FSR}}{dp'_T} \right) dp'_T \right\} \quad (3.28)$$

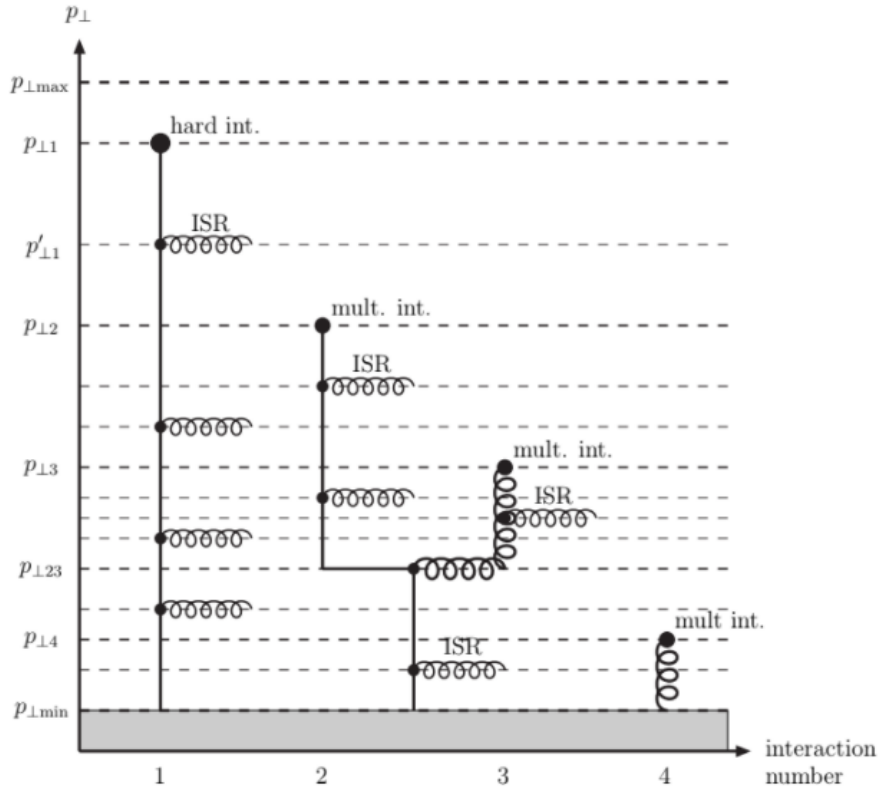


Figure 3.4: An example of Multiple Partons Interactions and associated radiations. The downward evolution in p_T is shown here by reading the graph from top to bottom. The 4 parton-parton interactions occur to p_{T1} , p_{T2} , p_{T3} and p_{T4} .

In Fig. 3.4 are shown 4 parton-parton interactions with their associated showers (ISR and FSR). The downward evolution correspond to read the graph from top to bottom. The first hard interaction occurs at a scale $p_T = p_{T1}$ while the following ones at lower scales p_{T2} , p_{T3} , p_{T4} . Each interaction is associated with its radiation the first one occurs at $p_T = p'_{T1}$. The scatterings at p_{T2} and p_{T3} are originating from the same mother parton.

This diagram is related to one of the two hadrons. The full event can be illustrated if a similar diagram is drawn for the other hadron and connected to the full black circles.

3.2.7 Beam Beam Remnants and primordial k_T

What is left after that the evolution is end?

The evolution in p_T can create an arbitrary complicate final state. This final state contains contributions from the scattered and unscattered partons that don't enter the p_T evolution. The last are the so called *Beam Beam Remnants* (BBR). BBR take into account the number of valence quarks remaining and the number of sea quarks required for the overall flavour conservation.

To ensure momentum conservation the BBR have to take all the remaining longitudinal momentum that is not extracted by the MPI initiators.

Primordial k_T

We have considered only the longitudinal momentum. In a real scenario partons, inside the hadrons, are fermions. So, are expected to have a non zero initial transverse momentum arising from the Fermi motion inside the incoming hadrons. This is denoted as *primordial k_T* . This is different from the transverse momentum derived from DGLAP shower evolution or from the hard interaction.

Based on Fermi motion alone, one would expect a value of the primordial k_T of the order of:

$$k_T \simeq \frac{\hbar}{r_p} \approx \frac{0.2 \text{ GeV} \cdot \text{fm}}{0.7 \text{ fm}} \approx 0.3 \text{ GeV} \quad , \quad (3.29)$$

but, as an example, to reproduce the data for the p_T distributions of Z bosons produced in hadron-hadron collisions, one need a larger contribution. This phenomenon has not a satisfactory phenomenological explanation. Until a convincing explanation is found the idea is to consider an effective primordial k_T for the initiators larger than the one in Eq. 3.29.

In **Pythia** the primordial k_T is assigned to initiators sampling a Gaussian distributions for p_x and p_y independently with variable width σ

$$\sigma(Q, \hat{m}) = \frac{Q_{1/2} \sigma_{\text{soft}} + Q \sigma_{\text{soft}}}{Q_{1/2} + Q} \frac{\hat{m}}{\hat{m}_{1/2} + \hat{m}} \quad (3.30)$$

Where Q is the hard-process renormalization scale for the main hard process and the p_T scale for subsequent MPI. σ_{soft} , σ_{hard} are the minimum and maximum width, \hat{m} is the invariant mass, while $Q_{1/2}$ and $\hat{m}_{1/2}$ the halfway values between the two extremes.

3.2.8 Color Reconnection and Hadronization

The last important step at parton level is the *color reconnection*. Color reconnection is motivated by the fact that MPI leads to different color strings. In the previous steps the planar limit of the QCD was assumed where $N_c \rightarrow \infty$. Now, moving to real case where $N_c = 3$ all this strings that can be overlapped in physical space can be reconnected. The basic idea is to reconnect strings in order to reduce the total string length; and thus the potential energy (Lund Model).

In PYTHIA8 the reconnection is performed giving to each system a probability to reconnect given by:

$$\mathcal{P}_{\text{rec}} = \frac{p_{T\text{rec}}^2}{(p_{T\text{rec}}^2 + p_T^2)} \quad p_{T\text{rec}} = R \times p_{T0} \quad , \quad (3.31)$$

the `ColorReconnection:range` R is a user-tunable parameter while p_{T0} is the same parameter defined in MPI simulation.

With this definition for the probability, it is clear that system with low p_T are more likely reconnected to other. This idea find is justification in the fact that lower p_T values correspond to larger spatial extension and so these strings have more chance to overlap with other and so to reconnect.

Hadronization

The hadronization takes all these partons (color strings) and transforms them in a set of color-neutral hadrons. Hadronization is based solely on the *Lund string fragmentation model* [27, 28].

Lund model basic idea is to break the color line and to reduce the total string length, the string is representative of the potential

$$V(r) = -\frac{a}{r} + \kappa r \quad \text{with} \quad \kappa \approx 1 \text{ GeV/fm} \quad , \quad (3.32)$$

where κ is the string tension. This potential is a combination of an attractive (Coulomb) potential and a linear potential that phenomenologically include quarks confinement. The linear potential is the dominating part at increasing distance values, so the energy increase with distance.

The simplest case is the one in Fig. 3.5: The $q\bar{q}$ system evolves in space increasing the string length at some point the distance is too large and is convenient to break the string into two strings.

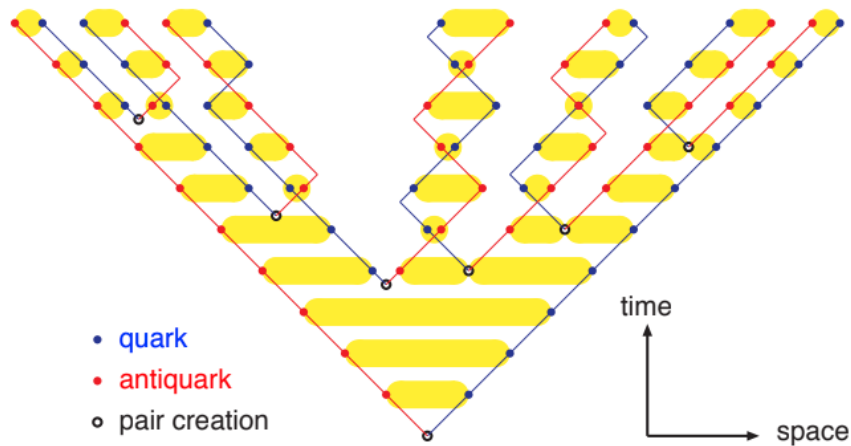


Figure 3.5: The lund Model is schematically shown here. The string evolution in time is shown vertically while the spatial position horizontally. As the partons move apart at some point become convenient to break the string, in order to reduce the total potential energy, and a partons pair is produced.

The hadronization step confines the quark into hadrons, then these hadrons can undergoes to hadron rescattering and decay. These are the hadrons that are revealed by the detectors.

3.3 PYTHIA summary

To summarize PYTHIA8 is able to simulate high energy hadron-hadron collisions. The evolution of the system is simulated in a common decreasing- p_T sequence the master formula for the evolution is written in Eq. 3.28.

This evolution start from an hard scale that is the scale of the main parton hard scattering that is described by a fixed ME calculation, PYTHIA can be interfaced with external frameworks for the ME step as POWHEG and MAD-GRAPE5 AMC@NLO. Then the parton shower is started with the simulation of ISR, FSR and MPI also the parton rescattering is allowed. Once the evolution is ended the hadronization transform the partons in a set of final hadrons these hadron than decay and rescatters against each others before the detection.

All these processes are describe mainly by phenomenological model, due to the not-known-by-first-principles soft QCD description. The use of these phenomenological models introduces lots of free parameters (some are been pointed out in the previously sections) that have to be tuned with data to give to PYTHIA the ability of simulate real events.

In the next chapter we are going to focus on the study of the underlying event and so on all the soft events related to an hard scattering in an hadron-hadron collision.

Bibliography

- [1] Steven Weinberg. A model of leptons, Nov 1967. URL <https://link.aps.org/doi/10.1103/PhysRevLett.19.1264>.
- [2] J. D. Bjorken. Asymptotic Sum Rules at Infinite Momentum. *Phys. Rev.*, 179: 1547–1553, 1969. doi: 10.1103/PhysRev.179.1547.
- [3] Sidney D Drell and Tung-Mow Yan. Partons and their applications at high energies, 1971. ISSN 0003-4916. URL <https://www.sciencedirect.com/science/article/pii/0003491671900716>.
- [4] J M Campbell, J W Huston, and W J Stirling. Hard interactions of quarks and gluons: a primer for lhc physics, Dec 2006. ISSN 1361-6633. URL <http://dx.doi.org/10.1088/0034-4885/70/1/R02>.
- [5] L N Lipatov. The parton model and perturbation theory, 1975. URL <http://cds.cern.ch/record/400357>.
- [6] Vladimir Naumovich Gribov and L N Lipatov. Deep inelastic ep scattering in perturbation theory, 1972. URL <https://cds.cern.ch/record/427157>.
- [7] G. Altarelli and G. Parisi. Asymptotic freedom in parton language, 1977. ISSN 0550-3213. URL <https://www.sciencedirect.com/science/article/pii/0550321377903844>.
- [8] Yuri L. Dokshitzer. Calculation of the Structure Functions for Deep Inelastic Scattering and $e^+ e^-$ Annihilation by Perturbation Theory in Quantum Chromodynamics., 1977.
- [9] W.J. Stirling. private communication. URL <http://www.hep.ph.ic.ac.uk/~wstirling/plots/plots.html>.
- [10] F. Bloch and A. Nordsieck. Note on the radiation field of the electron, Jul 1937. URL <https://link.aps.org/doi/10.1103/PhysRev.52.54>.
- [11] Toichiro Kinoshita. Mass singularities of feynman amplitudes, 1962. URL <https://doi.org/10.1063/1.1724268>.
- [12] T. D. Lee and M. Nauenberg. Degenerate systems and mass singularities, Mar 1964. URL <https://link.aps.org/doi/10.1103/PhysRev.133.B1549>.
- [13] A. Kulesza, G. Sterman, and W. Vogelsang. Electroweak vector boson production in joint resummation, 2002. URL <https://arxiv.org/abs/hep-ph/0207148>.

- [14] Torbjörn Sjöstrand, Stefan Ask, Jesper R. Christiansen, Richard Corke, Nishita Desai, Philip Ilten, Stephen Mrenna, Stefan Prestel, Christine O. Rasmussen, and Peter Z. Skands. An introduction to pythia 8.2, Jun 2015. ISSN 0010-4655. URL <http://dx.doi.org/10.1016/j.cpc.2015.01.024>.
- [15] Manuel Bähr, Stefan Gieseke, Martyn A. Gigg, David Grellscheid, Keith Hamilton, Oluseyi Latunde-Dada, Simon Plätzer, Peter Richardson, Michael H. Seymour, Alexander Sherstnev, and Bryan R. Webber. Herwig++ physics and manual, Nov 2008. ISSN 1434-6052. URL <http://dx.doi.org/10.1140/epjc/s10052-008-0798-9>.
- [16] T Gleisberg, S Hoeche, F Krauss, A Schaelicke, S Schumann, and J Winter. Sherpa 1. , a proof-of-concept version, Feb 2004. ISSN 1029-8479. URL <http://dx.doi.org/10.1088/1126-6708/2004/02/056>.
- [17] E. Boos, M. Dobbs, W. Giele, I. Hinchliffe, J. Huston, V. Ilyin, J. Kan-zaki, K. Kato, Y. Kurihara, L. Lonnblad, M. Mangano, S. Mrenna, F. Paige, E. Richter-Was, M. Seymour, T. Sjostrand, B. Webber, and D. Zeppenfeld. Generic user process interface for event generators, 2001.
- [18] Stefano Catani, Frank Krauss, Bryan R Webber, and Ralf Kuhn. Qcd matrix elements + parton showers. *Journal of High Energy Physics*, 2001(11):063–063, Nov 2001. ISSN 1029-8479. doi: 10.1088/1126-6708/2001/11/063. URL <http://dx.doi.org/10.1088/1126-6708/2001/11/063>.
- [19] Stefano Frixione and Bryan R Webber. Matching nlo qcd computations and parton shower simulations. *Journal of High Energy Physics*, 2002(06):029–029, Jun 2002. ISSN 1029-8479. doi: 10.1088/1126-6708/2002/06/029. URL <http://dx.doi.org/10.1088/1126-6708/2002/06/029>.
- [20] Stefano Frixione, Paolo Nason, and Bryan R Webber. Matching nlo qcd and parton showers in heavy flavour production. *Journal of High Energy Physics*, 2003(08):007–007, Aug 2003. ISSN 1029-8479. doi: 10.1088/1126-6708/2003/08/007. URL <http://dx.doi.org/10.1088/1126-6708/2003/08/007>.
- [21] Stefano Frixione and Bryan R. Webber. The mc@nlo 3.1 event generator, 2005.
- [22] Rikkert Frederix and Stefano Frixione. Merging meets matching in MC@NLO. *JHEP*, 12:061, 2012. doi: 10.1007/JHEP12(2012)061.
- [23] Victor S. Fadin. BFKL resummation. *Nucl. Phys. A*, 666:155–164, 2000. doi: 10.1016/S0375-9474(00)00022-1.
- [24] I. I. Balitsky and L. N. Lipatov. The Pomeranchuk Singularity in Quantum Chromodynamics. *Sov. J. Nucl. Phys.*, 28:822–829, 1978.
- [25] Richard D. Ball, Valerio Bertone, Stefano Carrazza, Luigi Del Debbio, Stefano Forte, Patrick Groth-Merrild, Alberto Guffanti, Nathan P. Hartland, Zahari Kassabov, José I. Latorre, Emanuele R. Nocera, Juan Rojo, Luca Rottoli,

- Emma Slade, and Maria Ubiali. Parton distributions from high-precision collider data. *The European Physical Journal C*, 77(10), Oct 2017. ISSN 1434-6052. doi: 10.1140/epjc/s10052-017-5199-5. URL <http://dx.doi.org/10.1140/epjc/s10052-017-5199-5>.
- [26] FRANK SIEGERT. Monte-carlo event generation for the lh, 2010. URL <http://etheses.dur.ac.uk/484/>.
- [27] B. Andersson, G. Gustafson, G. Ingelman, and T. Sjöstrand. Parton fragmentation and string dynamics. *Physics Reports*, 97(2):31–145, 1983. ISSN 0370-1573. doi: [https://doi.org/10.1016/0370-1573\(83\)90080-7](https://doi.org/10.1016/0370-1573(83)90080-7). URL <https://www.sciencedirect.com/science/article/pii/0370157383900807>.
- [28] Torbjorn Sjostrand. Jet Fragmentation of Nearby Partons. *Nucl. Phys. B*, 248: 469–502, 1984. doi: 10.1016/0550-3213(84)90607-2.
- [29] Underlying Event Measurements with Leading Particles and Jets in pp collisions at $\sqrt{s} = 13$ TeV. Technical report, CERN, Geneva, 2015. URL <https://cds.cern.ch/record/2104473>.
- [30] Serguei Chatrchyan et al. Measurement of the underlying event in the Drell-Yan process in proton-proton collisions at $\sqrt{s} = 7$ TeV. *Eur. Phys. J. C*, 72: 2080, 2012. doi: 10.1140/epjc/s10052-012-2080-4.
- [31] A. M. Sirunyan et al. Measurement of the underlying event activity in inclusive Z boson production in proton-proton collisions at $\sqrt{s} = 13$ TeV. *JHEP*, 07:032, 2018. doi: 10.1007/JHEP07(2018)032.
- [32] Albert M. Sirunyan et al. Study of the underlying event in top quark pair production in pp collisions at 13 TeV. *Eur. Phys. J. C*, 79(2):123, 2019. doi: 10.1140/epjc/s10052-019-6620-z.
- [33] Florian Bechtel. *The underlying event in proton-proton collisions*. PhD thesis, Hamburg U., 2009.
- [34] Albert M Sirunyan et al. Extraction and validation of a new set of CMS PYTHIA8 tunes from underlying-event measurements. *Eur. Phys. J. C*, 80(1):4, 2020. doi: 10.1140/epjc/s10052-019-7499-4.
- [35] Andy Buckley, Hendrik Hoeth, Heiko Lacker, Holger Schulz, and Jan Eike von Seggern. Systematic event generator tuning for the LHC. *Eur. Phys. J. C*, 65: 331–357, 2010. doi: 10.1140/epjc/s10052-009-1196-7.
- [36] Marco Lazzarin, Simone Alioli, and Stefano Carrazza. MCNNTUNES: Tuning Shower Monte Carlo generators with machine learning. *Comput. Phys. Commun.*, 263:107908, 2021. doi: 10.1016/j.cpc.2021.107908.
- [37] Martín Abadi, Ashish Agarwal, Paul Barham, Eugene Brevdo, Zhifeng Chen, Craig Citro, Greg S. Corrado, Andy Davis, Jeffrey Dean, Matthieu Devin, Sanjay Ghemawat, Ian Goodfellow, Andrew Harp, Geoffrey Irving, Michael Isard, Yangqing Jia, Rafal Jozefowicz, Lukasz Kaiser, Manjunath Kudlur, Josh

- Levenberg, Dandelion Mané, Rajat Monga, Sherry Moore, Derek Murray, Chris Olah, Mike Schuster, Jonathon Shlens, Benoit Steiner, Ilya Sutskever, Kunal Talwar, Paul Tucker, Vincent Vanhoucke, Vijay Vasudevan, Fernanda Viégas, Oriol Vinyals, Pete Warden, Martin Wattenberg, Martin Wicke, Yuan Yu, and Xiaoqiang Zheng. TensorFlow: Large-scale machine learning on heterogeneous systems, 2015. URL <https://www.tensorflow.org/>. Software available from tensorflow.org.
- [38] F. Rosenblatt. The perceptron: A probabilistic model for information storage and organization in the brain. 1958. URL <https://doi.org/10.1037/h0042519>.
- [39] Kurt Hornik. Approximation capabilities of multilayer feedforward networks. *Neural Networks*, 4(2):251–257, 1991. ISSN 0893-6080. doi: [https://doi.org/10.1016/0893-6080\(91\)90009-T](https://doi.org/10.1016/0893-6080(91)90009-T). URL <https://www.sciencedirect.com/science/article/pii/089360809190009T>.
- [40] Moshe Leshno, Vladimir Ya. Lin, Allan Pinkus, and Shimon Schocken. Multilayer feedforward networks with a nonpolynomial activation function can approximate any function. *Neural Networks*, 6(6):861–867, 1993. ISSN 0893-6080. doi: [https://doi.org/10.1016/S0893-6080\(05\)80131-5](https://doi.org/10.1016/S0893-6080(05)80131-5). URL <https://www.sciencedirect.com/science/article/pii/S0893608005801315>.
- [41] Nikolaus Hansen. The CMA evolution strategy: A tutorial. *CoRR*, abs/1604.00772, 2016. URL <http://arxiv.org/abs/1604.00772>.
- [42] G. Cowan. *Statistical data analysis*. Oxford University Press, USA, 1998.